Changes in Atmospheric Blocking Circulations Linked with Winter Arctic Warming: A New Perspective

DEHAI LUO AND XIAODAN CHEN

Key Laboratory of Regional Climate-Environment for Temperate East Asia, Institute of Atmospheric Physics, Chinese Academy of Sciences, Beijing, China

AIGUO DAI

Department of Atmospheric and Environmental Sciences, University at Albany, State University of New York, Albany, New York

IAN SIMMONDS

School of Earth Sciences, University of Melbourne, Melbourne, Victoria, Australia

(Manuscript received 25 January 2018, in final form 7 June 2018)

ABSTRACT

Winter atmospheric blocking circulations such as Ural blocking (UB) have been recognized to play an important role in recent winter Eurasian cooling. Observational analyses performed here reveal that the winter warming in the Barents–Kara Seas (BKS) related to the recent decline of sea ice concentration (SIC) has been accompanied by a large increase in the mean duration of the UB events. A new energy dispersion index (EDI) is designed to help reveal the physics behind this association and show how the BKS warming can influence the mean duration of UB events. This EDI mainly reflects the role of the meridional potential vorticity (PV) gradient in the blocking persistence and it characterizes the changes in energy dispersion and nonlinearity strength of blocking. The meridional PV gradient combines the relative vorticity gradient (related to the nonuniform meridional shear of the mean zonal wind) and the mean zonal wind strength. It is revealed that the BKS warming leads to a significant lengthening of the UB duration because of weakened energy dispersion and intensified nonlinearity of the UB through reduced meridional PV gradient. Furthermore, the duration of the UB is found to depend more strongly on the meridional PV gradient than the mean westerly wind strength, although the meridional PV gradient includes the effect of mean westerly wind strength. Thus, the meridional PV gradient is a better indicator of the change in the blocking duration related to Arctic warming than the zonal wind strength index.

1. Introduction

In the past three decades, the winter sea ice concentration (SIC) in the Arctic, especially in the Barents–Kara Seas (BKS), has undergone a rapid decline (Stroeve et al. 2005; Comiso 2006; Francis and Hunter 2007; Serreze et al. 2007; Simmonds 2015), which often corresponds to a large Arctic warming (Graversen et al. 2008; Overland et al. 2008; Screen and Simmonds 2010). In recent years, the impact of the SIC decline and Arctic warming on midlatitude atmospheric circulations has become an important research topic because continental cold anomalies are often linked to the winter Arctic sea ice loss or Arctic warming through changes in atmospheric circulations (Overland et al. 2011; Outten and Esau 2012; Screen and Simmonds 2013; Cohen et al. 2014; Mori et al. 2014; Vihma 2014; Simmonds and Govekar 2014; Kug et al. 2015; Luo et al. 2016a,b; Shepherd 2016; Yao et al. 2017).

Atmospheric blocking is a quasi-stationary midlatitude large-scale circulation pattern with a lifetime of 10–20 days (Diao et al. 2006). It has been recognized to play a key role in transporting cold air from high to middle latitudes, thus affecting short-term weather and climate in the mid-to-high latitudes (Rex 1950; Scherrer et al. 2006; Tyrlis and Hoskins 2008). Thus, establishing a link between northern midlatitude blocking and Arctic warming is key for understanding how the Arctic warming and SIC decline affect midlatitude cold extremes (Cohen et al. 2014).

Corresponding author: Dr. Dehai Luo, ldh@mail.iap.ac.cn

DOI: 10.1175/JCLI-D-18-0040.1

Previously, numerous one-dimensional (1D) and two-dimensional (2D) blocking indices have been used to examine climatological features of atmospheric blocking activities (Dole and Gordon 1983; Tibaldi and Molteni 1990; Diao et al. 2006; Scherrer et al. 2006; Anderson et al. 2017). However, how the midlatitude blocking is linked to Arctic warming during the recent decades is still an open question, although the enhanced Arctic warming is expected to weaken meridional temperature gradients, which may weaken midlatitude westerlies (Yao et al. 2017) and midlatitude jet streams (Newson 1973; Francis and Vavrus 2012, 2015; Barnes and Screen 2015; Hassanzadeh and Kuang 2015). These changes are expected to have substantial impacts on midlatitude blocking.

Newson (1973) was the first to use a numerical model experiment to suggest that the ice-free Arctic can increase the incidence of blocking events due to the reduced westerly winds caused by weakened temperature gradients associated with enhanced Arctic warming. More recently, a series of studies indicated that winter Artic warming can influence the planetary waves and the Arctic Oscillation (AO) through changes in the westerlies (Murray and Simmonds 1995; Francis and Vavrus 2012, 2015; Walsh 2014; Semenov and Latif 2015; Hassanzadeh and Kuang 2015). In particular Francis and Vavrus (2012, 2015) and Walsh (2014) suggested that the recent Arctic warming tends to slow down the zonal winds and promote the meandering of a westerly jet and thus enhance meridional winds. In essence, the meandering westerly jet corresponds to a blocking flow and thus the previous work on blocking can be applied to this case (Luo 2000, 2005; Luo and Li 2000; Luo et al. 2014). In fact, the Arctic warming changes not only the strength of the mid-tohigh-latitude mean zonal wind (Francis and Vavrus 2015) but also its spatial structure (Luo et al. 2016a; Yao et al. 2017). However, it is unclear whether the change in the spatial structure (e.g., nonuniform meridional shear) of mean westerly winds related to Arctic warming is important for changes in the blocking duration and frequency, although the weakening of the midlatitude zonal wind strength appears to be an important element for blocking maintenance (Newson 1973; Francis and Vavrus 2015; Yao et al. 2017). Thus, evaluating the relative contributions of the strength and nonuniform meridional shear of the mean westerly wind associated with Arctic warming to the blocking duration change can improve understanding of the impact of Arctic warming on midlatitude weather. Recently, Luo et al. (2016a) found that an atmospheric response to the winter BKS SIC decline or warming is manifested as a large-scale wave train that is comprised of Ural blocking (UB) and the positive phase of the North Atlantic Oscillation (NAO^+). This suggests that the BKS warming likely favors persistent and quasi-stationary UB events (Yao et al. 2017). However, how the winter BKS warming changes the mean duration of the UB events has not been quantified to date. Specifically, it is unclear which physical processes dominate the influence of the BKS warming on the duration of the UB. In this paper we present a new approach aimed at revealing why the BKS warming associated with the sea ice decline can prolong the lifetime of UB events via the construction and analysis of a new circulation index.

This paper is organized as follows: In section 2, we describe the data, index, and method. We also describe a nonlinear multiscale interaction model to motivate us to put forward an energy dispersion perspective. In section 3, the energy dispersion of the blocking in a slowly varying nonzonal flow is described using the linear potential vorticity (PV) equation. The results on the roles of reduced meridional PV gradient and mid-to-high-latitude zonal wind strength in the lengthening of the UB duration are presented in section 4. The conclusion and discussions are summarized in the final section.

2. Data, index, and method

a. Data and identification method of blocking events

Winter [December–February (DJF)] daily atmospheric and sea ice data were taken from the ERA-Interim on a 2.5° × 2.5° grid (Dee et al. 2011). The variables we used include SIC, surface air temperature (SAT), 500-hPa geopotential height (Z500), and horizontal winds for the period from December 1979–February 1980 to December 2016–February 2017 (1979–2016). The anomaly of each variable at each grid point is defined as its deviation from the 1979–2016 mean for each calendar day.

We used the one-dimensional blocking index developed by Tibaldi and Molteni (1990) (TM) to identify blocking events. The TM index is based on the reversal of the Z500 gradients: $\mathrm{GHGS} = [\mathrm{Z500}(\phi_0) - \mathrm{Z500}(\phi_S)]/(\phi_0 - \phi_S)$ and $\mathrm{GHGN} = [\mathrm{Z500}(\phi_N) - \mathrm{Z500}(\phi_0)]/(\phi_N - \phi_0)$ at three specific latitudes: $\phi_0 = 60°\mathrm{N} + \Delta$, $\phi_N = 80°\mathrm{N} + \Delta$, and $\phi_S = 40°\mathrm{N} + \Delta$ for $\Delta = -5°$, 0°, and 5° latitude. A large-scale blocking is defined if there are $\mathrm{GHGS} > 0$ and $\mathrm{GHGN} < -10\,\mathrm{gpm}\,(°\,\mathrm{lat})^{-1}$ for any one of the three values of Δ, and they persist for at least three consecutive days (a 3-day threshold). The same blocking definition can also be made for at least five consecutive days or a 5-day threshold. A blocking event is identified as an UB if it occurs within the 30°–90°E longitudinal sector. In this paper, the 3- and 5-day thresholds are used to identify UB events to make a comparison, though the frequency of blocking events is lower for the 5-day threshold, as mentioned in Scherrer et al. (2006). Moreover, because

the TM index cannot better reflect the length of blocking duration (10–20 days), we will quantify the duration of a blocking event using its domain-averaged height anomaly. Specifically, we define the duration of an UB event as the number of days when the daily Z500 anomaly averaged over the region 55°–75°N, 30°–90°E exceeds 80 gpm during its life cycle. In addition, we used the 2D blocking index, the absolute geopotential height (AGP) index suggested by Scherrer et al. (2006), to examine the sensitivity of our results to different blocking indices. For comparison, the UB events are also identified using the 5-day threshold of the AGP index in the region of 50°–75°N, 30°–90°E.

b. *A nonlinear multiscale interaction model of blocking events*

Many previous studies have indicated that the forcing of transient synoptic-scale eddies plays an important role in the blocking maintenance (Berggren et al. 1949; Shutts 1983; Illari and Marshall 1983; Hoskins et al. 1983; Vautard and Legras 1988). Because earlier theoretical models (Charney and DeVore 1979; McWilliams 1980) could only describe the time-mean structure of blocking patterns and failed to depict the life cycle of a blocking event, it is difficult to use these models to examine how Arctic warming may change blocking duration, strength, and movement. Luo (2000, 2005), Luo and Li (2000), and Luo et al. (2014) proposed and developed a nonlinear multiscale interaction (NMI) model to describe the life cycle of a blocking dipole with a 10–20-day time scale by considering the blocking–eddy interaction. Although this NMI model is highly idealized and only considers a uniform westerly wind prior to the block onset, it still provides an efficient tool for further examining how Arctic warming may affect the blocking. In this NMI model, the blocking is mainly driven by preexisting incident synoptic-scale eddies upstream, even though some of the blocking events arise from the propagation of upstream planetary wave trains (Luo et al. 2016b). Actually, this NMI model can also describe the formation of wave train–induced blocking even in the absence of preexisting synoptic eddies. Because the blocking has an approximate barotropic structure, the barotropic PV equation, which has been also widely used to explore the blocking dynamics (Charney and DeVore 1979; McWilliams 1980), may be used to examine our problem. In this paper, we use the barotropic NMI model and neglect the effect of vertical shear of mean zonal winds or baroclinicity on blocking. Thus, it is useful to briefly describe the analytical solution of this NMI model to motivate our new perspective on how Arctic warming may change blocking. Under a prior uniform westerly wind u_0, the analytical solution of the nondimensional planetary-scale field ψ_P (i.e., barotropic streamfunction) of an eddy-driven blocking from the barotropic PV equation of the NMI model, scaled by the characteristic wind speed $\tilde{U} = 10\,\mathrm{m\,s^{-1}}$ and length $\tilde{L} = 1000\,\mathrm{km}$, in a β-plane channel can be obtained as (Luo and Li 2000; Luo 2005; Luo et al. 2014, 2018)

$$\psi_P = -u_0 y + \psi \approx -u_0 y + \psi_B + \psi_m, \tag{1a}$$

$$\psi_B = B\sqrt{\frac{2}{L_y}}\exp[i(kx-\omega t)]\sin(my) + \mathrm{cc}, \tag{1b}$$

$$\psi_m = -|B|^2 \sum_{n=1}^{\infty} q_n g_n \cos(n+1/2)my, \quad \text{and} \tag{1c}$$

$$i\left(\frac{\partial B}{\partial t} + C_g\frac{\partial B}{\partial x}\right) + \lambda\frac{\partial^2 B}{\partial x^2} + \delta|B|^2 B + Gf_0^2\exp[-i(\Delta kx - \Delta\omega t)] = 0, \tag{1d}$$

where $\omega = kC_p$, $C_p = u_0 - (\beta + Fu_0)/(k^2 + m^2 + F)$, $|B|^2 = BB^*$, and $C_g = \partial\omega/\partial k = u_0 - (\beta + Fu_0)(m^2 + F - k^2)/(k^2 + m^2 + F)^2$; $\lambda = [3(m^2 + F) - k^2](\beta + Fu_0)k/(k^2 + m^2 + F)^3$ is the linear dispersion term; $\delta = \delta_N/(\beta + Fu_0)$ is the nonlinearity strength of the blocking with $\delta_N > 0$ (see the appendix); ψ_B is the streamfunction anomaly of the blocking; ψ_m is the streamfunction of the mean westerly wind change; B is the blocking amplitude with a complex conjugate B^*; β is the nondimensional meridional gradient of the Coriolis parameter; cc denotes the conjugate of its preceding term; $F = (\tilde{L}/R_d)^2$, where R_d is the radius of Rossby deformation; k and m are the zonal and meridional wavenumbers of the blocking anomaly, respectively; f_0 is the amplitude distribution of preexisting incident synoptic-scale eddies; and L_y is the width of the β-plane channel. Note that δ_N of δ is given in the appendix and the mathematical expressions of G, $\Delta\omega$, and Δk can be found in Luo et al. (2018).

While the blocking is generated by the forcing of synoptic-scale eddies (Berggren et al. 1949; Shutts 1983), the blocking anomaly ψ_B can be described by a linear barotropic PV equation to the first-order approximation (Luo and Li 2000; Luo 2005), and its amplitude B satisfies the nonlinear Schrödinger equation [Eq. (1d)]. Although the numerical solution of Eq. (1d) can give the time evolution of a blocking pattern for a given initial condition and parameters (Luo 2005; Luo et al. 2014), here we do not seek the evolution solution of a blocking, instead we only use Eqs. (1a)–(1d) to construct our energy dispersion perspective.

c. *The energy dispersion and nonlinearity of blocking and their link to the north–south PV gradient*

We see in Eq. (1) that $C_p = \omega/k$ is the phase speed, and C_g is the group velocity of the blocking if the wave amplitude represents the energy of blocking. We also note that the linear dispersion term λ is proportional to $\beta + Fu_0$, but the nonlinearity strength δ is proportional to $1/(\beta + Fu_0)$.

It is easy to show that $\lambda\partial^2 B/\partial x^2$ and $\delta|B|^2B$ are small, and $i(\partial B/\partial t + C_g\partial B/\partial x) \approx 0$ in the absence of eddy forcing when B and its higher-order variation are small. Under such a condition, which is satisfied in a linear framework or during the early period prior to blocking onset, the blocking anomaly has a solution of $\psi_B = B(x - C_g t)\sqrt{2/L_y}\exp[ik(x - C_p t)]\sin(my) + \text{cc}$. This allows us to examine whether the blocking system will have a strong or weak dispersion if the magnitude of $C_g - C_p$ can be known. The blocking is nearly nondispersive and long-lived if there is $C_g \approx C_p$ even when it is amplified by the eddy forcing (Luo 2000). Thus, it is concluded that whether the blocking system has a weak dispersion or a long lifetime is mainly determined by the difference between its C_g and C_p ($C_{\text{gp}} = C_g - C_p$). We obtain $C_{\text{gp}} = C_g - C_p = 2k^2(\beta + Fu_0)/(k^2 + m^2 + F)^2$ for a uniform background westerly wind u_0.

In the real atmosphere, the mean westerly wind is usually slowly varying in the meridional direction. Thus, here we extend our NMI model to the case of a slowly varying zonal flow. For a given slowly varying zonal flow U, the β term is modified as $\beta - \partial^2 U/\partial y^2$ by the nonuniform meridional shear $\partial^2 U/\partial y^2$ of the basic zonal flow U. In this case, $\beta + Fu_0$ in the coefficients of Eq. (1d) should be replaced by $\beta - \partial^2 U/\partial y^2 + FU$ and u_0 should be replaced by U. Because the meridional PV gradient $\text{PV}_y = \partial\text{PV}/\partial y = \beta - \partial^2 U/\partial y^2 + FU$ for a slowly varying zonal flow U, then C_p, C_g, λ, and δ in Eqs. (1a)–(1d) should be $C_p = U - \text{PV}_y/(k^2 + m^2 + F)$, $C_g = U - \text{PV}_y(m^2 + F - k^2)/(k^2 + m^2 + F)^2$, $\lambda = \text{PV}_y[3(m^2 + F) - k^2]k/(k^2 + m^2 + F)^3$, and $\delta = \delta_N/\text{PV}_y$. For this case, one can also obtain $C_{\text{gp}} = 2k^2\text{PV}_y/(k^2 + m^2 + F)^2$ under such a condition.

It is further found that λ and C_{gp} are proportional to PV_y, but δ is proportional to $1/\text{PV}_y$ for $\text{PV}_y \neq 0$ in a nonlinear framework. On this basis, we can understand whether the blocking system has a weak dispersion and a strong nonlinearity or a long lifetime if PV_y can be known for a given slowly varying zonal flow prior to the blocking onset. Thus, the magnitude of PV_y determined by the background flow prior to the blocking onset may be used as a measure of the blocking duration, as it determines C_{gp}, which in turn controls the energy dispersion rate and the lifetime of a blocking event as stated above.

It should be pointed out that because $\text{PV}_y = \beta + Fu_0$ for a uniform background westerly wind u_0, PV_y is small and the blocking can maintain its long lifetime in higher latitudes or in weaker westerly wind regions because of β or u_0 being small. This may explain why blocking events tend to occur in higher latitudes (Yeh 1949) or in the regions with weak zonal winds such as Eurasia. However, under some conditions, the decrease in the nonuniform meridional shear $-\partial^2 U/\partial y^2$ of the zonal wind seems to be more important for the weakening of PV_y than the reduction in mean westerly wind strength, as noted below. This suggests that the nonuniform meridional shear of the zonal wind is important for the energy dispersion of blocking and its lifetime. In particular, the blocking will have weak dispersion and strong nonlinearity, and hence a long lifetime when PV_y is small. To some extent, the small PV gradient may be considered as a weak PV barrier that favors cold-air intrusion from the Arctic to midlatitudes through increasing the blocking persistence.

Previously, Francis and Vavrus (2012) and Walsh (2014) argued that the Arctic warming could slow down the planetary waves because of the weakening of mean westerly wind strength through reduced meridional temperature gradient based on the phase speed of linear Rossby waves like $C_p = U - \beta/(k^2 + m^2)$, although a clear slowdown of the midlatitude jet stream and westerlies is not evident in observations or future model projections (Barnes and Polvani 2015; Barnes and Screen 2015). However, the slowing down of the planetary wave or blocking does not imply that it has a long lifetime. In this paper, we emphasize that the magnitude of PV_y is crucial for the lifetime of blocking. Below, we will indicate that the Arctic warming can change the duration of blocking through changing the magnitude of PV_y associated with the strength and horizontal structure of mean westerly winds.

3. Effects of Arctic warming on blocking: An energy dispersion perspective

It is suggested (e.g., Francis and Vavrus 2012; Walsh 2014) that mid-to-high-latitude winds may become less zonal with more meridional flows as the Arctic warming occurs under rising greenhouse gases (GHGs). Here, we will evaluate the effect of meridional flows on the blocking duration by including meridional winds in the PV equation. As revealed above, because C_{gp}, λ, and nonlinearity δ show opposite variations with PV_y, it is sufficient to calculate C_{gp} only (instead of both λ and δ) in a slowly varying nonzonal flow to reflect the changes in the nonlinearity and dispersion of a blocking system. As demonstrated by Luo (2005), the blocking anomaly satisfies a linear PV equation to the first-order approximation, while the amplitude of the blocking anomaly is shown to satisfy a nonlinear Schrödinger equation that is derived from high-order approximation equations. Thus, here we may still use a linear PV equation to derive the mathematical expression of C_{gp} in a slowly varying nonzonal flow. For a blocking perturbation superimposed on a slowly varying nonzonal flow (U, V), the nondimensional linear barotropic vorticity equation is expressed as

$$\left(\frac{\partial}{\partial t}+U\frac{\partial}{\partial x}+V\frac{\partial}{\partial y}\right)(\nabla^2\psi'-F\psi')+(\zeta_y+FU)\frac{\partial\psi'}{\partial x}+(VF-\zeta_x)\frac{\partial\psi'}{\partial y}=0, \quad (2)$$

where ψ' is the perturbation streamfunction, F is the same as defined above, $\zeta_y=\beta+Q_y$ is the meridional gradient of the nondimensional absolute vorticity $\zeta=\beta y+Q$ with respect to y, and $\zeta_x=Q_x$ is its zonal gradient with respect to x. Here $Q=\partial V/\partial x-\partial U/\partial y$ is the relative vorticity, and the mean streamfunction ψ satisfies $U=-\partial\psi/\partial y$ and $V=\partial\psi/\partial x$, where U and V are the mean zonal and meridional winds, respectively.

Using the Wentzel–Kramers–Brillouin (WKB) method (Nayfeh 2000), from Eq. (2) it is easy to obtain the dispersion relation of a blocking perturbation with a waveform of $\exp[i(kx+my-\omega t)]$ for an infinite β-plane approximation as

$$\omega=kU+mV-\frac{(\zeta_y+FU)k+(FV-\zeta_x)m}{k^2+m^2+F}. \quad (3)$$

In a barotropic atmosphere without forcing, because the PV can be expressed as $\mathrm{PV}=\zeta-F\psi=\beta y+Q-F\psi$, we can have $\mathrm{PV}_y=\beta+Q_y+FU$ and $\mathrm{PV}_x=Q_x-FV$. Thus, it is found that the PV gradients are not only related to the absolute or relative vorticity gradients, but also horizontal winds. As noted above, whether the blocking strongly disperses its energy depends on the difference between its group velocity $C_g=\partial\omega/\partial k$ and phase speed $C_p=\omega/k$. Thus, the energy dispersion of the blocking can be characterized by

$$C_{\mathrm{gp}}=C_g-C_p=-\frac{m}{k}V+\frac{2k^2\mathrm{PV}_y}{(k^2+m^2+F)^2}-\frac{m}{k}\mathrm{PV}_x\frac{(3k^2+m^2+F)}{(k^2+m^2+F)^2}.$$

It is found that the mathematical expression of C_{gp} reduces to the case of a slowly varying zonal flow U as presented above when both V and PV_x are small. Given this form, it is helpful to define

$$\langle C_{\mathrm{gp}}\rangle=-\frac{m}{k}\langle V\rangle+\frac{2k^2}{(k^2+m^2+F)^2}\langle\mathrm{PV}_y\rangle-\frac{m}{k}\frac{(3k^2+m^2+F)}{(k^2+m^2+F)^2}\langle\mathrm{PV}_x\rangle$$

as a measure of domain-averaged energy dispersion to characterize the change of the blocking duration related to Arctic warming, where the angle brackets denote a domain average over a region within the blocking and its adjacent region. Because the magnitude of $\langle C_{\mathrm{gp}}\rangle$ reflects the energy dispersion of blocking and thus the length of the blocking duration, $\langle C_{\mathrm{gp}}\rangle$ suggests that the blocking duration is related to not only the meridional and zonal gradients of the PV, but also the meridional wind. However, because $\langle V\rangle\approx0$ and $\langle\mathrm{PV}_x\rangle\approx0$, as we shall establish below, $\langle C_{\mathrm{gp}}\rangle$ can be further approximated as $\langle C_{\mathrm{gp}}\rangle\approx2k^2\langle\mathrm{PV}_y\rangle/(k^2+m^2+F)^2$. Correspondingly, we can also have $\langle C_p\rangle\approx\langle U\rangle-\langle\mathrm{PV}_y\rangle/(k^2+m^2+F)$. These expressions show that the energy dispersion of the blocking is proportional to $\langle\mathrm{PV}_y\rangle$, whereas its movement depends on both the zonal wind strength and $\langle\mathrm{PV}_y\rangle$. In this case, we can define a simplified domain-averaged energy dispersion index (EDI), $\mathrm{EDI}=\langle\mathrm{PV}_y\rangle$. Hence, the simple model results suggest that the blocking duration is mainly determined by $\langle\mathrm{PV}_y\rangle$.

In fact, the meridional PV gradient reflects the combination of the meridional relative vorticity gradient and the zonal wind strength because $\mathrm{PV}_y=\beta+Q_y+FU$. Thus, the Arctic warming influences the meridional PV gradient likely through changing the zonal winds in strength and horizontal structure (or meridional inhomogeneity). But previous studies only considered the effect of the mean zonal wind strength change (Newson 1973; Francis and Vavrus 2015; Yao et al. 2017). Because there is $\mathrm{PV}_y\approx\beta-\partial^2U/\partial y^2+FU$ for a slowly varying zonal flow U, we conclude that $\partial^2U/\partial y^2$ can play a more important role in the blocking duration change when U is weaker. This condition is easily satisfied in the Eurasian mid-to-high latitudes where the zonal winds are often weak (Yao et al. 2017). In fact, the occurrence of blocking requires a weak background westerly wind (Luo et al. 2014). It is also found that the PV_y is mainly determined by the strength of zonal winds only when $|\partial^2U/\partial y^2|\ll|FU|$. This case corresponds to a strong PV_y and hence a strong energy dispersion, which occurs in the strong westerly wind regions of North Pacific and North Atlantic midlatitudes and suppresses atmospheric blocking as a barrier. However, over Eurasia, the mean zonal wind (U) is relatively weak and the $\partial^2U/\partial y^2$ term cannot be neglected. Thus, the physical meaning of this EDI is different from the previous index of Francis and Vavrus (2012, 2015), who only emphasized the role of the wind strength change. In contrast, our $\mathrm{EDI}=\langle\mathrm{PV}_y\rangle$ considers the combined effect of the mean zonal wind strength and the nonuniform meridional shear of the mean zonal wind that may be altered by Arctic warming.

4. Results

a. *Impact of warming in BKS on the duration of UB*

Because the strongest warming in winter occurs in the BKS as a result of large SIC loss (Luo et al. 2016a), in

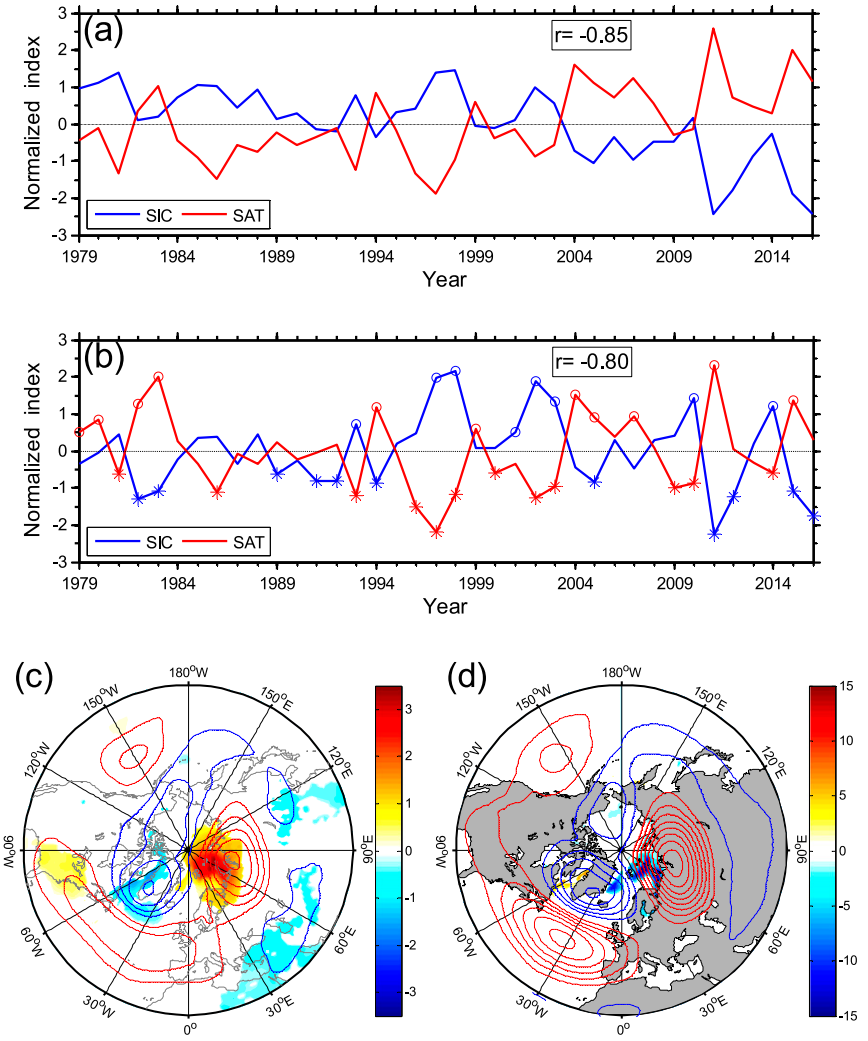

FIG. 1. Time series of the normalized winter-mean SIC (blue) and SAT (red) anomalies averaged over the BKS (65°–85°N, 30°–90°E) for (a) nondetrended and (b) detrended data, where the circles and asterisks denote ±5 STD. (c) Regressed Z500 [contour interval (CI) = 5 gpm STD^{-1}] and SAT (color shading; K STD^{-1}) anomalies against the detrended BKS SIC time series during 1979–2016; and (d) regressed Z500 (CI = 5 gpm STD^{-1}) and SIC (color shading; % STD^{-1}) anomalies against the time series of the detrended SAT anomaly averaged over the BKS.

this study we focus on examining the link between the BKS warming and UB. Here, we first establish a connection between the BKS SIC decline and warming and show in Figs. 1a and 1b the time series of the winter-mean SIC and SAT anomalies averaged over the BKS region (65°–85°N, 30°–90°E) for nondetrended (Fig. 1a) and detrended (Fig. 1b) data. While the domain-averaged SIC in the BKS region has strong negative correlations of −0.80 and −0.85 ($p \leq 0.01$) with the domain-averaged SAT for detrended (Fig. 1b) and nondetrended (Fig. 1a) data, the decreased trend of the BKS SIC is followed by an increased trend of the BKS SAT (Fig. 1a). Some studies indicated that the SIC loss can enhance the BKS warming through increased surface heat fluxes (Screen and Simmonds 2010) even though the atmospheric circulation pattern is absent. In Fig. 1c we show the regressed fields of the DJF Z500 and SAT anomalies against the DJF domain-averaged BKS SIC time series, whereas Fig. 1d shows the regressed fields of DJF Z500 and SIC anomalies against the BKS SAT time series. Figure 1 reveals that the BKS warming can correspond to a SIC decline and an UB together with a NAO^+ (Luo et al. 2016a,b). Thus, the BKS warming related to the SIC decline is accompanied by UB. However, it is unknown whether and by how much the BKS warming changes the duration of the UB.

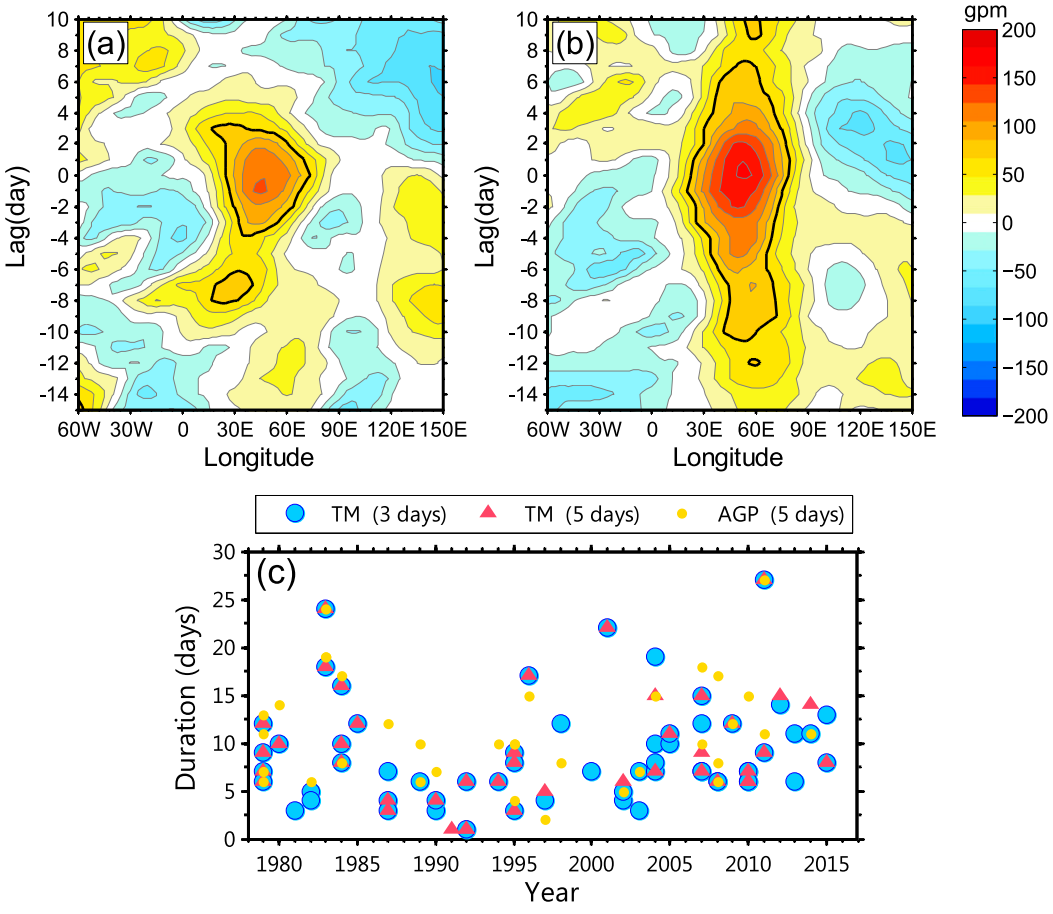

FIG. 2. Time–longitude evolution of composite daily Z500 anomalies averaged over the region 50°–75°N of UB events in (a) cold and (b) warm BKS winters for the detrended data, where the thick black solid contour denotes the value of 80 gpm. (c) Time series of the duration of UB events in winter during 1979–2016 identified with the 3- (blue circle) and 5-day (red triangle) threshold TM indices and 5-day threshold AGP index (yellow dot).

While the UB and BKS warming are often coupled together, we can investigate this further by looking at the difference of the UB between warm and cold BKS winters and changes in background conditions for nonblocking events. The winters when the normalized domain-averaged BKS SAT anomaly has a value equal to or larger than 0.5 standard deviation (STD) are defined as warm BKS winters, which include the 1979 (i.e., for December 1979–February 1980), 1980, 1982, 1983, 1994, 1999, 2004, 2005, 2007, 2011, and 2015 winters in Fig. 1b. Analogously, the cold BKS winters are defined as SAT ≤ -0.5 STD, and include the 1981, 1986, 1993, 1996, 1997, 1998, 2000, 2002, 2003, 2009, 2010, and 2014 winters.

During 1979–2016 winters, there are 58 (42) UB events identified by the TM index with a 3-day (5 day) duration threshold. But 35 UB events are identified when the 5-day threshold AGP index of Scherrer et al. (2006) is used. Below, we mainly use these UB events identified with a 3-day threshold TM index because the 5-day threshold easily leaves out short-lived blocking events (Scherrer et al. 2006). We further find that there are 20 (15) UB events in warm (cold) BKS winters for the 3-day threshold TM index. But a comparison between the TM and AGP indices is based on a 5-day duration threshold. Such a treatment has two advantages: One is that we can compare the results of the TM index between 3- and 5-day thresholds; and the other is that we can compare the difference of the result between 1D and 2D blocking indices with the same duration threshold.

We show the time–longitude evolution of the composite Z500 anomalies averaged over 50°–75°N for the 15 and 20 UB events in cold (Fig. 2a) and warm (Fig. 2b) BKS winters. The UB is less mobile and longer lasting in the warm BKS winters (Fig. 2b) than in the cold winters (Fig. 2a). Especially, the UB moves eastward during its growing phase and westward during its decay phase and

has a short lifetime during the cold BKS winter (Fig. 2a). The calculation shows that the UB has a mean duration of about 9 days in the cold BKS winters (Fig. 2a), compared with 18 days in the warm winters (Fig. 2b). Thus, an increase of about 100% in UB duration is a notable characteristic associated with the BKS warming. This result is also held even for nondetrended data (not shown). On the other hand, it is seen that the duration of UB was lower during the late 1980s and early 1990s than in preceding and subsequent years (Fig. 2c). The low duration of UB events in early 1990s sets the starting point for a subsequent upward trend in UB duration over a period that corresponds to BKS warming and SIC decline after the 1990s (Figs. 1a,b). This strongly suggests that the duration of UB depends on the BKS warming related to SIC decline. However, how Arctic warming may affect the duration of blocking is still unclear in previous studies (Luo et al. 2016a; Yao et al. 2017). Below we will demonstrate that a large increase in the UB duration is mainly related to the reduction of the meridional PV gradient induced by the BKS warming prior to the block onset, although the prior zonal wind strength can also influence the UB duration.

b. *Role of BKS warming in the meridional PV gradient and zonal wind changes*

Although the BKS warming is associated with prolonged UB, we cannot infer a causal relationship. Recent research (e.g., Luo et al. 2017; Lee et al. 2017) has highlighted the role of the BKS moisture intrusion and downward infrared radiation in these intricate connections. However, it is still unclear whether the BKS warming leads to changes in the UB or the opposite. This issue may be approached by examining if there are warming and positive height anomalies in BKS when the UB events are absent. Because the composite UB mainly occurs during a life cycle from lag −10 to 10 days around its peak (day 0; lag −10 or 10 day denotes the 10th day before or after the UB peak), the mean state for nonblocking events can be obtained by excluding blocking days from lag −10 to 10 days and calculating its time mean. We show the winter-mean Z500 and SAT anomalies in Figs. 3a and 3b for cold (Fig. 3a) and warm (Fig. 3b) BKS winters for nonblocking events. Figures 3c and 3d show the corresponding DJF-mean SIC anomalies in cold (Fig. 3c) and warm (Fig. 3d) BKS winters. It is found that positive temperature and height anomalies are still apparent in the BKS region in the warm BKS winters as a result of low SIC (Fig. 3d), even when the blocking days are excluded. But for the cold BKS winters only a negative height anomaly and cooling are seen in the BKS (Fig. 3a) as a result of high SIC (Fig. 3c) for nonblocking events. This suggests that the BKS warming exists because of the SIC decline in the absence of UB.

To some extent, the positive height anomaly and warming in BKS can be considered as a prior background condition under which the UB is developed and maintained. According to the PV theory of Hoskins et al. (1985), the warm (cold) temperature anomaly corresponds to a low (high) PV. Thus, it is speculated that the BKS warming cannot only weaken the zonal winds through reduced meridional temperature gradient (Newson 1973; Francis and Vavrus 2015; Yao et al. 2017), but also reduce the meridional PV gradient as the PV decreases in high latitudes because of high-latitude warming. Francis and Vavrus (2012, 2015) suggested that the reduction of midlatitude zonal winds can slow down the planetary waves. Here we further indicate that while the decline in meridional PV gradient and zonal winds can increase the UB duration, the reduced meridional PV gradient seems more important for the lengthening of the UB duration than the reduction of the mean zonal wind strength.

To quantify how the BKS warming related to SIC decline affects the UB through the change in the winter background state, we calculate the DJF-mean PV gradient and large-scale winds without blocking days for cold and warm BKS winters and compare their difference. For a blocking flow, we take $\tilde{L} \approx R_d$ (Luo et al. 2014), thus $F = (\tilde{L}/R_d)^2 \approx 1$ in Eq. (1). We also calculate the DJF mean U, V, Q_y, PV_y, and PV_x while the geostrophic wind is used to compute the relative vorticity gradient Q_y in $\zeta_y = \beta + Q_y$ of $\mathrm{PV}_y = \zeta_y + FU$ and $\tilde{U} = 10\,\mathrm{m\,s^{-1}}$ and $\tilde{L} = 1000\,\mathrm{km}$ are used. Because there is $\zeta_y = \beta + Q_y \approx \beta - U_{yy}$ prior to the blocking onset where $U_{yy} = \partial^2 U/\partial y^2$, it is useful to compare U and $-U_{yy}$ changes related to the BKS warming, while $-U_{yy}$ and U are closely related to the meridional temperature gradient change. On the other hand, because U_y represents the meridional shear of the mean zonal wind, $-U_{yy}$ reflects the nonuniform distribution of the meridional shear and is referred to as the nonuniform meridional shear of the mean zonal wind hereafter. As a result, the meridional PV gradient ($\mathrm{PV}_y \approx \beta - U_{yy} + FU$) can reflect the combined effect of the mean zonal wind strength and its nonuniform meridional shear.

Figure 4 shows the DJF-mean U, V, $-U_{yy}$, Q_y, PV_y, and PV_x for the cold and warm BKS winters excluding blocking days and also the warm minus cold winter difference. It is noted that between 50° and 70°N, U, $-U_{yy}$, Q_y, and PV_y are weaker east of 40°E in the warm BKS winters (Figs. 4b,h,k,q) than in the cold winters (Figs. 4a,g,j,p). This can be further seen from their difference fields (Figs. 4c,i,l,r). We also see that the meridional wind V (Figs. 4d,e) and PV_x (Figs. 4m,n) in the

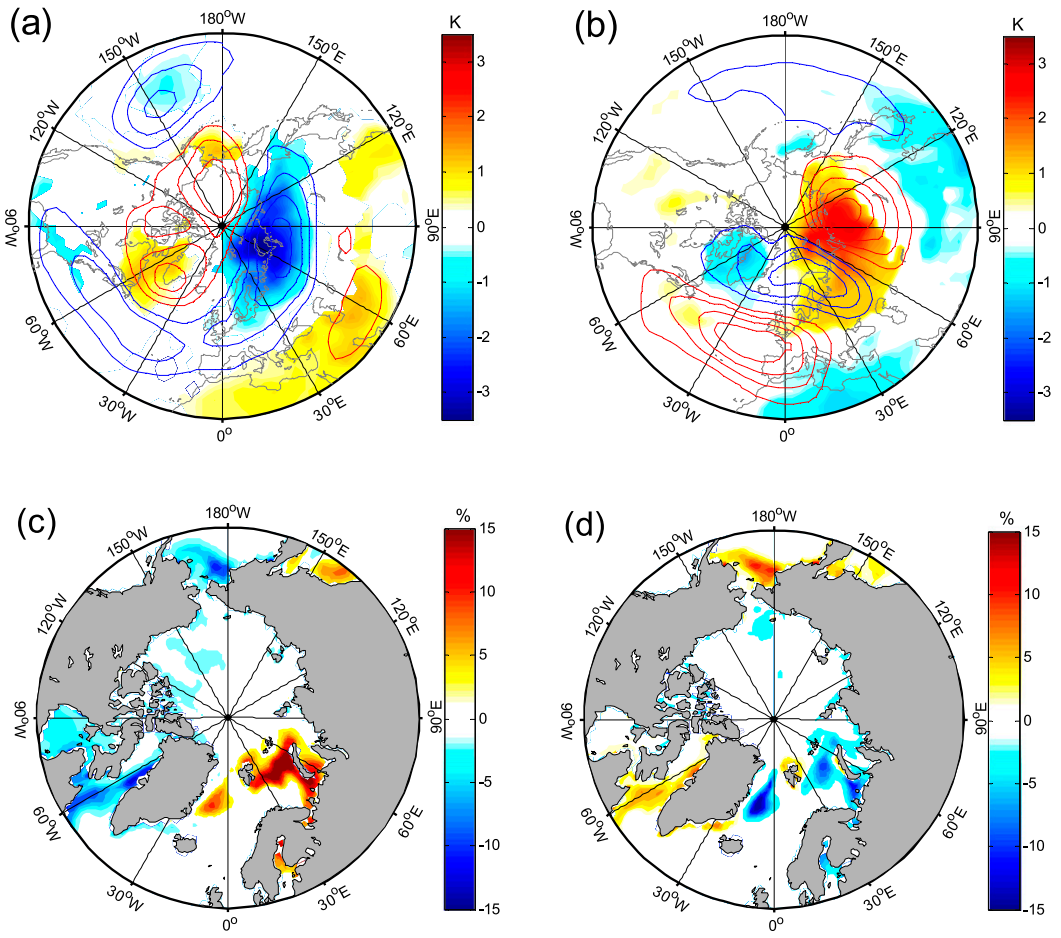

FIG. 3. Winter-mean detrended Z500 (CI = 10 gpm) and SAT (color shading) in (a) cold and (b) warm winters for nonblocking events (blocking days from lag −10 to 10 days are excluded and lag 0 denotes the blocking peak day). Winter-mean SIC anomaly in (c) cold and (d) warm winters for nonblocking events. The color shading represents the region above the 95% confidence level for the two-sided Student's t test.

region from 40° to 100°E and from 50° to 70°N are much smaller than the zonal wind U and PV_y, while V (PV_x) is increased (decreased) in the Eurasian high latitudes for warm BKS winters (Figs. 4e,n). Such a feature can clearly be seen from their warm minus cold winter difference (Figs. 4f,o). Because the UB originates from the east of 60°E in warm BKS winters, the choice of the average domain 55°–70°N, 40°–100°E is reasonable. Furthermore, we can show that their regional mean values of $\langle V\rangle$ and $\langle \mathrm{PV}_x\rangle$ averaged over the UB region (55°–70°N, 40°–100°E) are −0.13 and 0.01 (0.01 and −0.14) for the UB composite in cold (warm) BKS winters, respectively, which are much smaller than $\langle U\rangle$ and $\langle \mathrm{PV}_y\rangle$ with the values of 1.17 and 1.92 (0.99 and 1.38), and thus they can be neglected in $\langle C_{\mathrm{gp}}\rangle$ for $k \sim m$.

The domain-averaged Q_y ($-U_{yy}$) over 55°–70°N, 40°–100°E is 0.75 (0.54) in the cold BKS winters and 0.39 (0.31) for the warm BKS winters. Thus, the BKS warming corresponds to a decrease of about 48% (43%) in Q_y ($-U_{yy}$) in the Eurasian high latitudes. Such a Q_y decline corresponds to a decrease of 28% for $\langle \mathrm{PV}_y\rangle$ from 1.92 in the cold BKS winter to 1.38 in the warm BKS winter. The nondimensional U decreases by a more modest 15%, changing from 1.17 in cold BKS winters to 0.99 in warm BKS winters. The results above show that the decrease in the meridional PV gradient is significant because of BKS warming, and it is induced mainly by change in the $-U_{yy}$ term of relative vorticity, while the zonal wind strength reduction is also evident.

We also see that the decrease of $-U_{yy}$ is nearly 3 times that of the U reduction. But the decrease of $\langle \mathrm{PV}_y\rangle$ is about 2 times that due to the U reduction because $\mathrm{PV}_y \approx \beta - U_{yy} + FU$ considers the joint effect of $-U_{yy}$ and U. Thus, the role of Arctic warming tends to weaken the nonuniform meridional shear of the mean zonal wind besides reducing the mean zonal wind strength. In other words, the Arctic (or BKS) warming tends to cause a trend toward the PV homogenization ($\mathrm{PV}_y \approx 0$) over

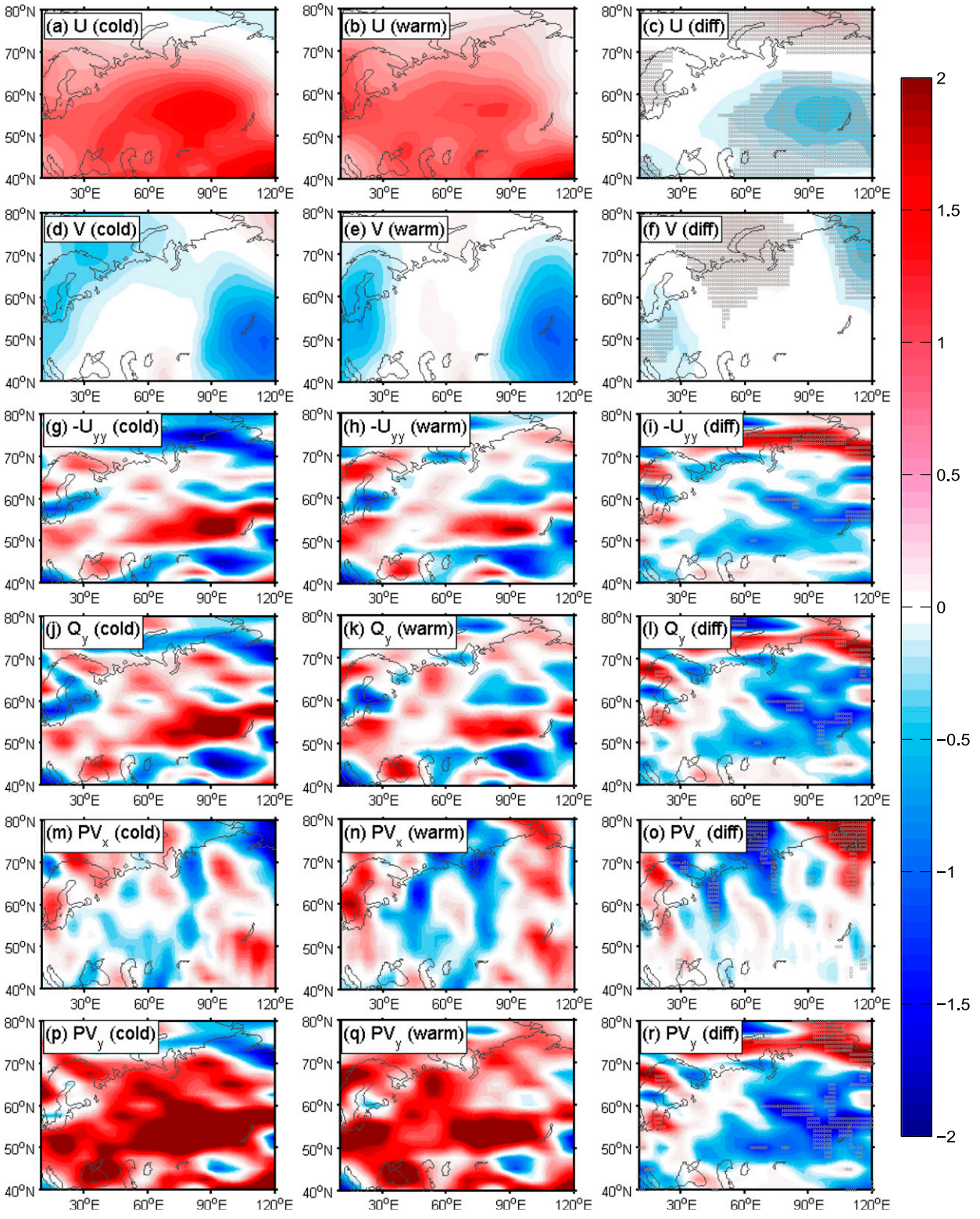

FIG. 4. Winter-mean nondimensional 500-hPa (a)–(c) U, (d)–(f) V, (g)–(i) $-U_{yy}$, (j)–(l) Q_y, (m)–(o) PV$_x$, and (p)–(r) PV$_y$ for β excluded in (left) cold and (center) warm BKS winters for nonblocking events (blocking days from lag −10 to 10 days are excluded); and (right) their warm minus cold winter difference. The gray crosses in the difference plots highlight regions over which the differences differ significantly from zero ($p < 0.05$).

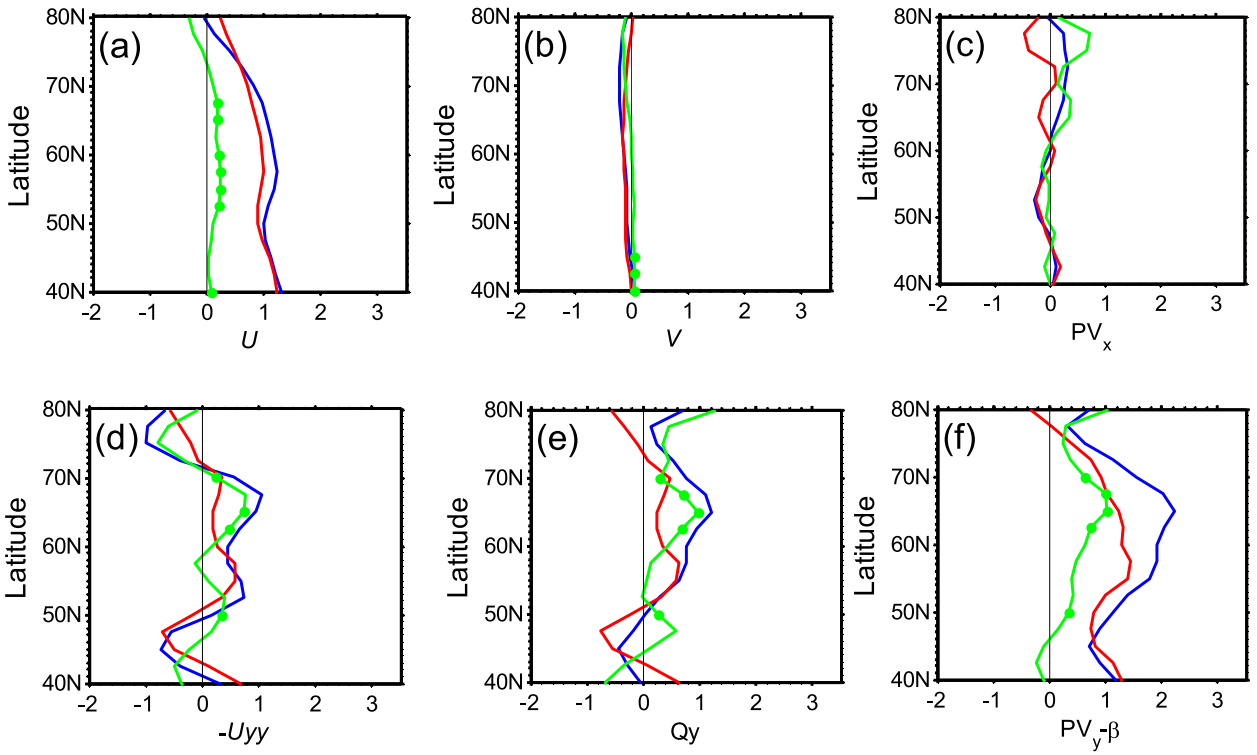

FIG. 5. Latitude cross sections of (a) U, (b) V, (c) PV_x, (d) $-U_{yy}$, (e) Q_y, and (f) $PV_y - \beta$ averaged in the longitude band 40°–100°E and from lag −20 to −10 days for UB events in warm (red; 20 UB cases in 11 winters) and cold (blue; 15 UB cases in 12 winters) BKS winters where lag 0 denotes the peak day of blocking and the green line denotes the cold minus warm winter difference. The dot represents their difference being significant at the 95% confidence level for a Monte Carlo test with 5000-times simulation.

Eurasia. In this case, we have a tendency toward $C_{gp} \approx 0$ so that the blocking tends to have a weak dispersion or a strong nonlinearity and hence a long-lasting persistence.

The warm minus cold winter difference fields of PV_y (Fig. 4r) and Q_y (Fig. 4l) show a structure similar to that of $-U_{yy}$ (Fig. 4i). This suggests that Q_y, or more specifically $-U_{yy}$, change contributes significantly to the variation of the PV_y field since $PV_y = \beta + Q_y + FU \approx \beta - U_{yy} + FU$. We also calculated the latitudinal cross sections of U, V, PV_x, $PV_y - \beta$, Q_y, and $-U_{yy}$ averaged over 40°–100°E and from lag −20 to −10 days prior to the UB peak (lag 0 day) and show the results in Figs. 5a–f for the warm and cold BKS winters. It is clear that the change of Q_y (Fig. 5e) or $-U_{yy}$ (Fig. 5d) is larger than the U change, especially at higher latitudes as the BKS warms up (Fig. 5a), whereas V (Fig. 5b) and PV_x (Fig. 5c) differences are very small in mid-to-high latitudes even V in the Arctic. Thus, the $-U_{yy}$ or Q_y change plays a more important role for the PV_y change (Fig. 5f) and thus UB duration than the U change (Fig. 5a).

To further examine how U, $-U_{yy}$, Q_y, and PV_y are linked to BKS warming through changing the meridional temperature gradient, it is useful to show the time series of DJF-mean U, $-U_{yy}$, Q_y, PV_y, BKS SAT, and meridional SAT gradient T_y during 1979–2016 winters in Fig. 6. Here, T_y is the SAT gradient between BKS and Eurasian midlatitudes and averaged over the region 50°–80°N, 40°–100°E as the meridional SAT gradient to reflect the role of BKS warming, while the values of U, $-U_{yy}$, Q_y, and PV_y are averaged over the region 55°–70°N, 40°–100°E. In our calculation we also exclude blocking events or blocking days to reflect the winter-mean state without the effect of blocking events. The correlation calculation (Table 1) shows that the meridional temperature gradient T_y and U in the UB region have correlation coefficients of 0.81 and −0.78 (0.72 and −0.54) with the BKS SAT, respectively, for raw (detrended) data (Fig. 6b), whereas T_y and U exhibit a negative correlation of −0.79 (−0.75). Such correlation coefficients, which are statistically significant ($p < 0.01$), imply that the BKS warming weakens the meridional temperature gradient to reduce mid-to-high-latitude zonal winds because there is $T_y > 0$ for a nonblocking case. We also see that while $-U_{yy}$, Q_y, and PV_y themselves have highly positive correlations (Fig. 6a), they show positive correlations with the BKS SAT and the meridional temperature gradient T_y, but significant negative correlations with the zonal wind strength U (Table 1). Thus, these results suggest that the BKS warming can weaken both the zonal wind strength U

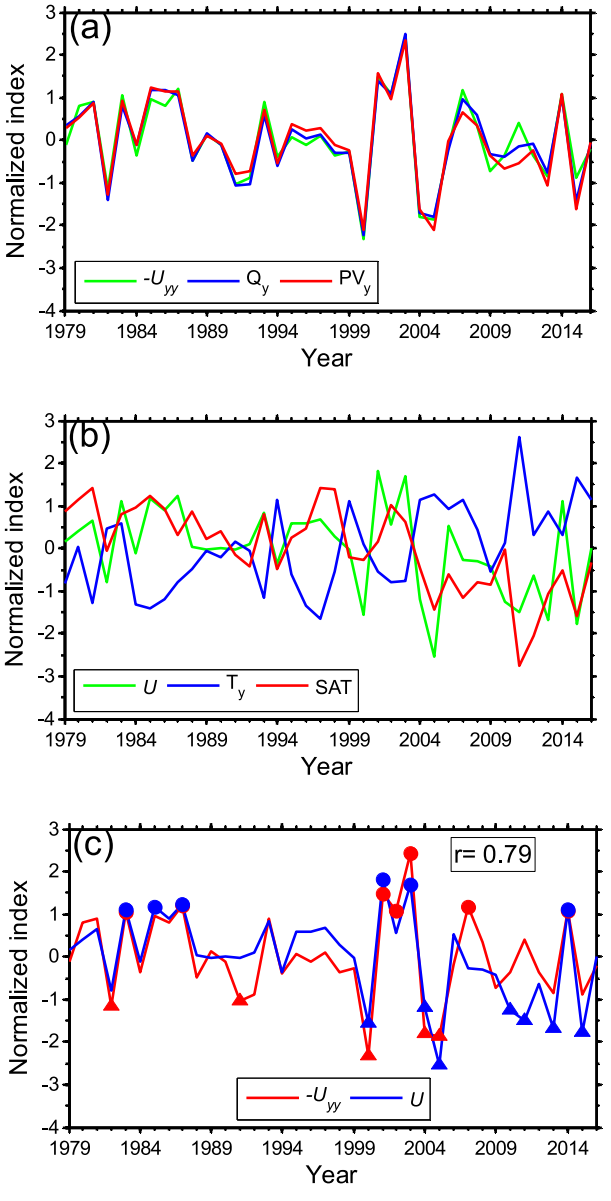

FIG. 6. Time series of normalized DJF-mean (a) Q_y, $-U_{yy}$, and PV_y; (b) U and T_y averaged over the UB region (55°–70°N, 40°–100°E) and SAT averaged over the BKS region; and (c) $-U_{yy}$ and U for nonblocking events (blocking days from lag −10 to 10 days are excluded) during 1979–2016, and their correlation coefficients are shown in Table 1. The dot (triangle) represents the value above (below) 1.0 (−1.0) STD.

and $-U_{yy}$ likely through the reduction of T_y, and thus the meridional relative vorticity gradient or meridional PV gradient. We also conclude that the decreases in $-U_{yy}$, Q_y, and PV_y are mainly attributed to the zonal wind changes in strength and spatial structure attributed to the reduced meridional temperature gradient.

Although $-U_{yy}$ is dependent on U and they have a correlation coefficient of 0.79 (0.80) ($p < 0.01$) for nondetrended (detrended) data, they reflect two different aspects of the mean westerly wind change. This is because $-U_{yy}$ is mainly linked to the nonuniform meridional shear of the mean westerly wind as noted above. The calculation (Fig. 6c) shows that for nondetrended raw data, the winters of the normalized DJF-mean $-U_{yy}$ (U) above 1.0 STD are 1983, 1987, 2001, 2002, 2003, 2007, and 2014 (1983, 1985, 1987, 2001, 2003, and 2014), but the winters of its value below −1.0 STD are 1982, 1991, 2000, 2004, and 2005 (2000, 2004, 2005, 2010, 2011, 2013, and 2015). Obviously, the winters of large or small $-U_{yy}$ are not identical to those of large or small U. In other words, some winters of large $-U_{yy}$ and U are not overlapped. Thus, $-U_{yy}$ and U are two different variables that represent the impact of BKS warming. This indicates that the EDI proposed here has a merit that the strength and nonuniform meridional shear of the mean zonal wind can be unified into a meridional PV gradient to describe how the BKS warming affects the blocking duration.

Of course, U, V, PV_x, $-U_{yy}$, $PV_y - \beta$, and Q_y vary with the blocking change because the mean winds are changed with the blocking evolution. For each blocking event, we can approximate the time-mean values of these variables prior to blocking onset as a background state of the blocking event. The calculation reveals that time-mean U, $-U_{yy}$, $PV_y - \beta$, and Q_y during the time period from lag −20 to −10 days prior to the UB onset are smaller in warm BKS winters than those in cold BKS winters (not shown). This suggests that a large decrease in the meridional PV gradient or westerly wind during the prior period of blocking is crucial for the long lifetime of the UB, while the prior meridional PV gradient reduction is likely more significant.

c. *Effects of reduced meridional PV gradient and zonal wind on the duration of UB*

To examine the impact of the prior horizontal wind and PV gradient strengths on the blocking duration, here we define the time mean of zonal and meridional winds averaged from lag −20 to −10 days as $\overline{U}$ and $\overline{V}$. Correspondingly, $-\overline{U_{yy}}$, $\overline{PV_x}$, $\overline{PV_y - \beta}$, and $\overline{Q_y}$ are used to represent the time-mean values of $-U_{yy}$, PV_x, $PV_y - \beta$, and Q_y averaged from lag −20 to −10 days.

Figures 7a–f show the scatter diagrams of the UB duration against domain-averaged $\langle\overline{U}\rangle$, $\langle\overline{V}\rangle$, $\langle-\overline{U_{yy}}\rangle$, $\langle\overline{PV_x}\rangle$, $\langle\overline{PV_y - \beta}\rangle$, and $\langle\overline{Q_y}\rangle$ over the region 55°–70°N, 40°–100°E for the 58 UB events diagnosed with a 3-day threshold TM index during all the winters from 1979 to 2016. It is found that the UB duration depends on the magnitudes of $\langle\overline{PV_y - \beta}\rangle$, $\langle\overline{Q_y}\rangle$, $\langle-\overline{U_{yy}}\rangle$, and $\langle\overline{U}\rangle$ prior to the UB onset, whereas the meridional wind $\langle\overline{V}\rangle$ (Fig. 7b) and zonal PV gradient $\langle\overline{PV_x}\rangle$ (Fig. 7c) have little effect on the UB duration because the slope between $\langle\overline{PV_x}\rangle$ or $\langle\overline{V}\rangle$ and the UB duration is small and not significant. We also see in Fig. 7 that some of the UB

TABLE 1. Correlation coefficients among DJF-mean $-U_{yy}$, Q_y, PV_y, and U averaged over the blocking region 55°–70°N, 40°–100°E, T_y averaged over the region 50°–80°N, 40°–100°E, and SAT and SIC averaged over the BKS region for nonblocking events. Here, the 95% (99%) confidence level with $p < 0.05$ ($p < 0.01$) for the t test is denoted by one asterisk (two asterisks).

Nondetrended (detrended)	Q_y	PV_y	SAT	T_y	U	SIC
$-U_{yy}$	0.97** (0.97**)	0.96** (0.96**)	−0.34* (−0.32*)	−0.46** (−0.48**)	0.79** (0.80**)	0.36* (0.36*)
Q_y		0.98** (0.99**)	−0.46** (−0.45**)	−0.50** (−0.52**)	0.81** (0.83**)	0.41** (0.42**)
PV_y			−0.53** (−0.49**)	−0.61** (−0.60**)	0.90** (0.91**)	0.50** (0.48**)
SAT				0.81** (0.72**)	−0.78** (−0.54**)	−0.82** (−0.71**)
T_y					−0.79** (−0.75**)	−0.78** (−0.59**)
U						0.65** (0.56**)

events have durations less than 3 days. This is because a weakness of the TM and AGP indices is that they can identify a strong large-scale low pressure trough south of a weak high ridge as a blocking in that these indices define a blocking event based on the reversal of the Z500 meridional gradient. Thus, some of the blocking events inevitably have durations less than the threshold required by the TM or AGP index if the persistence time

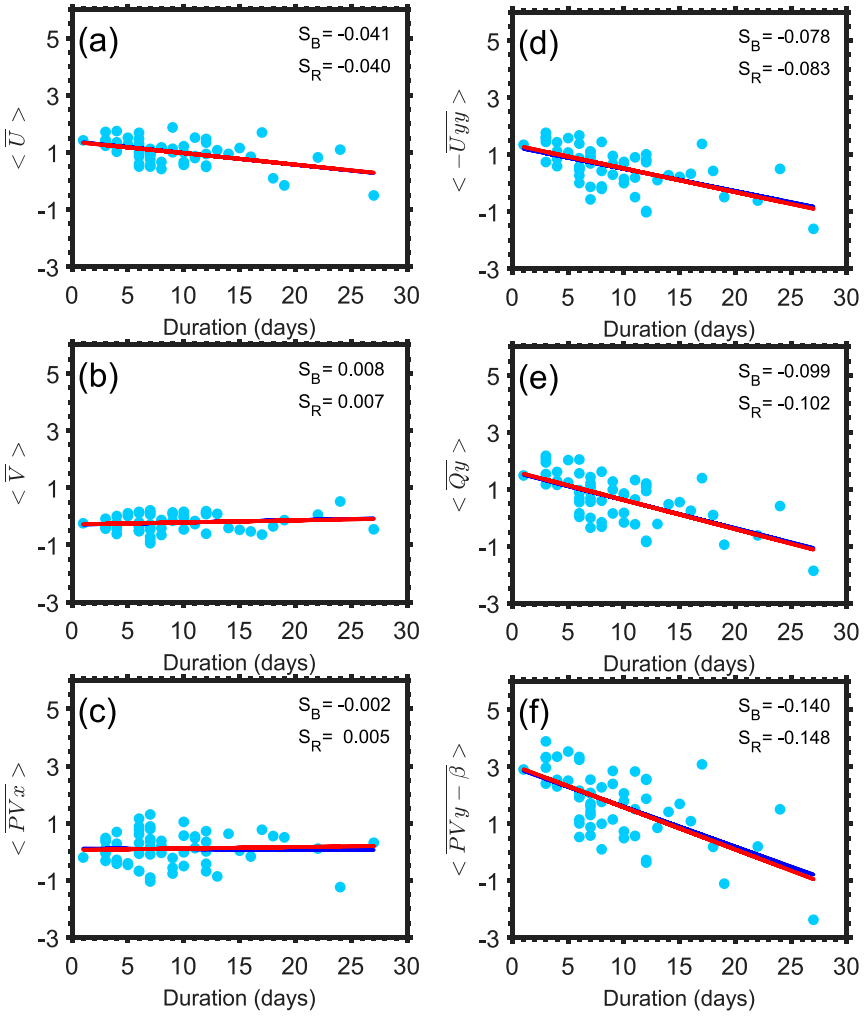

FIG. 7. Scatter diagrams of the UB duration against normalized (a) $\langle\overline{U}\rangle$, (b) $\langle\overline{V}\rangle$, (c) $\langle\overline{\mathrm{PV}_x}\rangle$, (d) $\langle-\overline{U_{yy}}\rangle$, (e) $\langle\overline{Q}_y\rangle$, and (f) $\langle\overline{\mathrm{PV}_y-\beta}\rangle$ for 58 UB events during the 1979–2016 winters, where S_B (blue line) represents the slope of least squares fitting straight line and S_R (red line) denotes that of the robust fitting straight line. The fitting lines in (a) and (d)–(f) are statistically significant at the 95% confidence level for the F test.

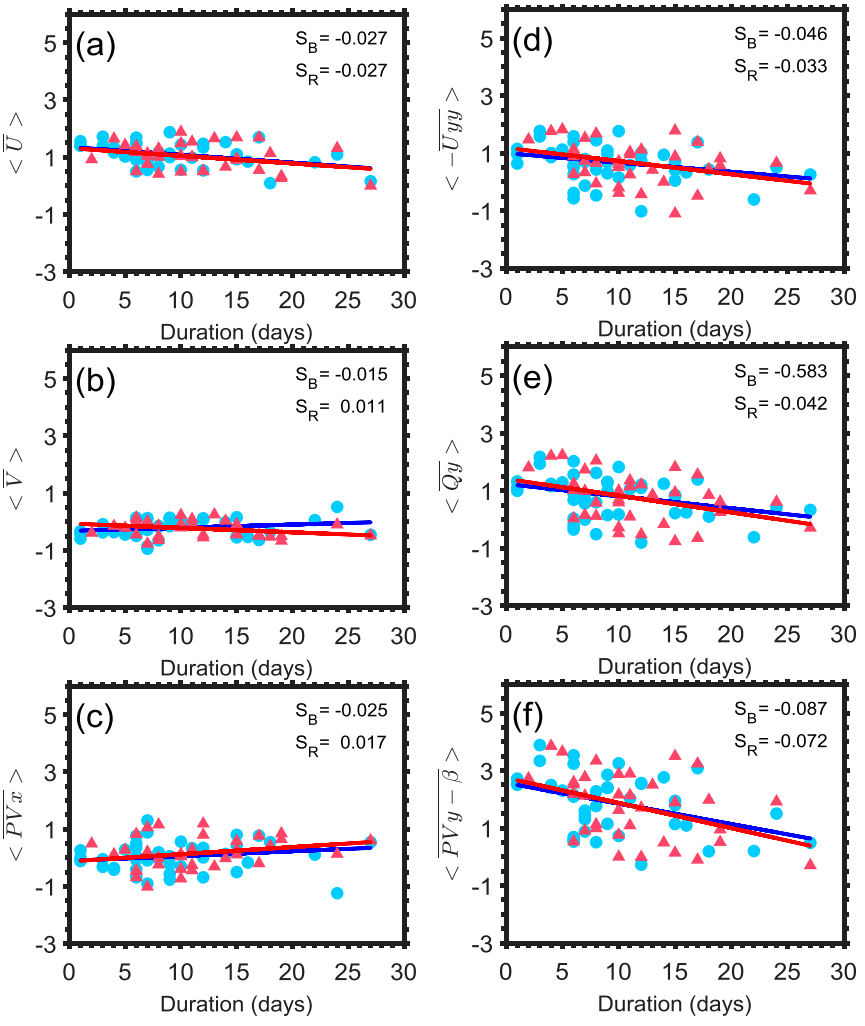

FIG. 8. Scatter diagrams of the UB duration against normalized (a) $\langle\overline{U}\rangle$, (b) $\langle\overline{V}\rangle$, (c) $\langle\overline{\mathrm{PV}_x}\rangle$, (d) $\langle-\overline{U_{yy}}\rangle$, (e) $\langle\overline{Q}_y\rangle$, and (f) $\langle\overline{\mathrm{PV}_y-\beta}\rangle$ for 42 (35) UB events during the 1979–2016 winters identified with a 5-day threshold TM (AGP) index, where S_B (blue line) represents the slope of robust fitting straight line for the 5-day threshold TM index and S_R (red line) denotes the result of the 5-day threshold AGP index. The fitting lines in (a) and (d)–(f) are statistically significant at the 95% confidence level for the F test.

over which the domain-averaged positive height anomaly north of the blocking pattern exceeds 80 gpm is defined as the duration of a blocking.

While the reduction of the mean zonal wind favors the increased UB duration (Fig. 7a), the decrease in the meridional PV gradient (Fig. 7f) or $\langle-\overline{U_{yy}}\rangle$ (Fig. 7d) or relative vorticity gradient $\langle\overline{Q}_y\rangle$ (Fig. 7e) seems to be more important for the lengthening of the UB than the westerly wind strength reduction (Fig. 7a), as the $\langle\overline{\mathrm{PV}_y-\beta}\rangle$-duration diagram shows a larger slope than that of the $\langle\overline{U}\rangle$-duration diagram. Especially, we find that the slope of the $\langle\overline{Q}_y\rangle$ or $\langle-\overline{U_{yy}}\rangle$ and the UB duration is about 2 times that of $\langle\overline{U}\rangle$, but the slope between $\langle\overline{\mathrm{PV}_y-\beta}\rangle$ and UB duration is about 3 times that of $\langle\overline{U}\rangle$. This means that while $\langle\overline{\mathrm{PV}_y-\beta}\rangle$, $\langle-\overline{U_{yy}}\rangle$, and $\langle\overline{U}\rangle$ changes work in the same direction, the contribution of the meridional PV gradient is about three times that of the westerly wind strength. Thus, the reduced meridional PV gradient has a dominant effect. We also test the sensitivity of the obtained results to the different blocking indices with a 5-day duration threshold. Similar results are found in Fig. 8 if both the 5-day threshold TM and AGP indices are used. In other words, our results are not sensitive to the different blocking indices and different duration thresholds. These results indicate that the increase in the UB duration depends more strongly on the reduction of the meridional PV gradient than the reduction of the mean westerly wind strength. Thus, the BKS warming related to the SIC loss

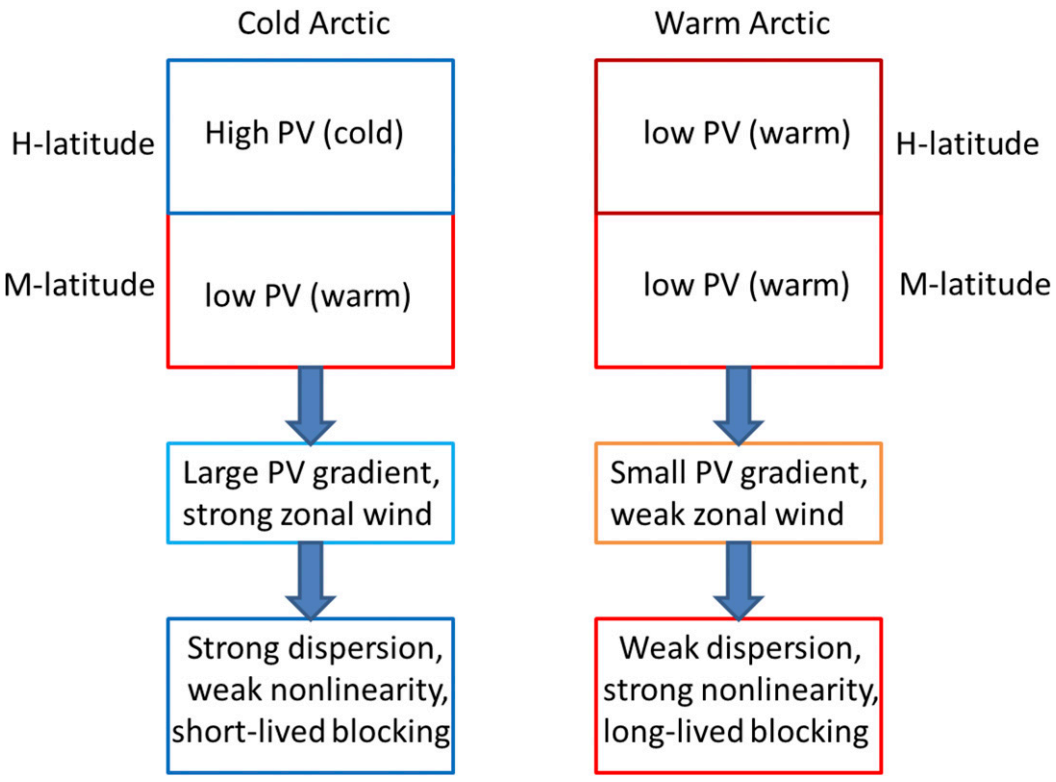

FIG. 9. Schematic diagram of the Arctic warming in BKS affecting the lifetime of UB, where the M-latitude (H-latitude) denotes the middle (high) latitude region, and the PV gradient represents PV_y.

can weaken the energy dispersion of the UB and enhance its nonlinearity and therefore prolong its lifetime mainly through the meridional PV gradient reduction. As noted above, the reduction of PV_y is not only related to the decrease in the mean westerly wind strength $\langle \overline{U} \rangle$, but also the reduction of the relative vorticity gradient related to the nonuniform meridional shear $\langle -\overline{U_{yy}} \rangle$ of the mean westerly wind. Thus, we present a new finding that the reduction of the meridional relative vorticity gradient related to the nonuniform meridional shear reduction of the mean zonal winds due to Arctic warming is likely more important for the increased persistence of blocking than the mean westerly wind strength reduction. This new finding differs from conclusions reached by previous studies, including Newson (1973), Outten and Esau (2012), Francis and Vavrus (2012, 2015), Walsh (2014), Luo et al. (2016a), and Yao et al. (2017), that focused on the role of reduced westerly wind strength related to Arctic warming in the slowing down of planetary waves and the increased duration of blocking.

5. Discussion and conclusions

The energy dispersion index proposed here provides a useful mathematical description of the links between the blocking duration and the meridional PV gradient that combines the meridional relative vorticity gradient (the nonuniform meridional shear of the mean zonal wind) and the mean zonal wind strength, which is related to the BKS warming associated with sea ice loss. It is revealed that the Arctic warming can significantly influence blocking mainly through the meridional PV gradient change rather than through the zonal PV gradient and meridional wind changes. In addition, we find that the EDI is mainly proportional to the meridional PV gradient PV_y. Because the energy dispersion and nonlinearity are two important processes intimately involved in the maintenance (duration) of the blocking, the EDI perspective, by means of the link between the BKS warming and meridional PV gradient, provides a clear understanding of how Arctic warming affects the blocking duration. It is found that the energy dispersion (nonlinearity) of blocking is proportional to PV_y ($1/PV_y$ for $PV_y \neq 0$). When the meridional PV gradient is weak because of BKS warming, the EDI is small. This means that the blocking is weakly dispersive and has a strong nonlinearity. In this case, the blocking can maintain itself for a longer period and have large amplitude because of the suppression of its energy dispersion. We can schematize our theoretical explanation of why BKS warming favors the long-lived UB in Fig. 9. It illustrates that the midlatitude Eurasian region has a low

PV and the high latitude has a high PV when the BKS in the Arctic is cold and the midlatitude continent is warm (Fig. 9, left). Correspondingly, the meridional PV gradient is large and the westerly wind is strong. For this case, the energy dispersion (nonlinearity) of the UB is strong (weak). Thus, the UB rapidly disperses its energy so that its lifetime is short under the cold Arctic condition. In this case, the strong PV gradient is a PV barrier that inhibits blocking and southward intrusion of associated cold air. In contrast, both the meridional PV gradient and midlatitude westerly winds are small when the BKS in the Arctic is warm as a result of the SIC loss (Fig. 9, right). The Arctic warming tends to produce a trend toward the PV homogenization ($PV_y \approx 0$) over Eurasia. As a result, the energy dispersion (nonlinearity) of the UB tends to be weak (strong), and the UB does not readily disperse its energy and hence can maintain its long life under the warm Arctic condition. Our results provide new thinking of how the midlatitude atmospheric circulations such as blocking are linked to Arctic warming associated with sea ice loss.

On the other hand, we have quantified the change in the duration of UB as the BKS warms up and the SIC decreases in winter. Because the meridional PV gradient is proportional to the meridional relative vorticity gradient and mean zonal wind strength, the recent BKS warming can weaken the meridional PV gradient because of reduced zonal winds through the reduced meridional temperature gradient. It is also found that the BKS warming can lead to a large increase in the UB mean duration. Moreover, our investigation has revealed that the reduction of the meridional PV gradient in the Eurasian midlatitudes due to BKS warming is more pronounced than the decrease in midlatitude westerly wind strength over Eurasia, though the meridional PV gradient includes the effect of the zonal wind strength change. Thus, the reduced meridional PV gradient is more important for the large increase in UB duration than the weakening of the westerly wind strength, whereas the westerly wind strength reduction plays a secondary role in the lengthening of UB. The effects of the reduced meridional PV gradient and zonal wind strength on the UB duration are about 3:1, as revealed in Figs. 7a and 7f. In short, the above results are new findings that differ from previous studies and provide a new perspective on how the Arctic warming and associated sea ice loss affect midlatitude atmospheric circulations. Of course, our new mechanism summarized in Fig. 9 may apply to summer blocking variability if the summer warming or sea ice decline is intense in the Arctic region (Hassanzadeh and Kuang 2015). This warrants further exploration.

It should be pointed out that the impact of the vertical shear of the mean zonal wind on the UB duration has been neglected in our model here, which focused on the different contributions of the mean zonal wind strength and the nonuniform meridional shear of the mean zonal wind to the blocking change. The effect of the vertical shear of the mean zonal wind on blocking has been examined in our previous study (Yao et al. 2017). Further investigations are needed to determine whether the meridional PV gradient is influenced by other factors and how the UB with strong or weak PV gradient affects the winter Eurasian temperatures or cold extremes. On the basis of this thinking about the PV gradient, the PV-barrier theory of the Arctic–midlatitude weather linkage will be presented in another paper.

Acknowledgments. The first two authors acknowledge the support from the National Natural Science Foundation of China (Grant 41430533) and Chinese Academy of Sciences Strategic Priority Research Program (Grant XDA 19070403). Dai was partly supported by the U.S. National Science Foundation (Grant AGS-1353740), U.S. Department of Energy's Office of Science (Award DE-SC0012602), and the U.S. National Oceanic and Atmospheric Administration (Award NA15OAR4310086). Simmonds was funded, in part, by Australian Research Council Grant DP160101997. The authors thank three anonymous reviewers for their very helpful suggestions that greatly improved the paper.

APPENDIX

The Nonlinearity Strength Coefficient of the Nonlinear Multiscale Interaction Model

The mathematical expression of δ_N in the nonlinearity strength δ in Eq. (1d) is

$$\delta_N = \frac{km\sum_{n=1}^{\infty} q_{Nn} g_n^2 [k^2 + m^2 - m^2(n+1/2)^2]}{k^2 + m^2 + F},$$

$$q_{Nn} = \frac{4k^2 m}{L_y\{1 - (m^2 + F - k^2)[F + m^2(n+1/2)^2]/(k^2 + m^2 + F)^2\}}, \quad \text{and}$$

$$g_n = \frac{8}{m[4 - (n+1/2)^2]L_y}.$$

REFERENCES

Anderson, B. T., P. Hassanzadeh, and R. Caballero, 2017: Persistent anomalies of the extratropical Northern Hemisphere wintertime circulation as an initiator of El Niño/Southern Oscillation events. *Sci. Rep.*, **7**, 10145, https://doi.org/10.1038/s41598-017-09580-9.

Barnes, E. A., and L. M. Polvani, 2015: CMIP5 projections of Arctic amplification, of the North American/North Atlantic circulation, and of their relationship. *J. Climate*, **28**, 5254–5271, https://doi.org/10.1175/JCLI-D-14-00589.1.

——, and J. A. Screen, 2015: The impact of Arctic warming on the midlatitude jet-stream: Can it? Has it? Will it? *Wiley Interdiscip. Rev.: Climate Change*, **6**, 277–286, https://doi.org/10.1002/wcc.337.

Berggren, R., B. Bolin, and C.-G. Rossby, 1949: An aerological study of zonal motion, its perturbations and break-down. *Tellus*, **1** (2), 14–37, https://doi.org/10.3402/tellusa.v1i2.8501.

Charney, J. G., and J. G. DeVore, 1979: Multiple flow equilibria in the atmosphere and blocking. *J. Atmos. Sci.*, **36**, 1205–1216, https://doi.org/10.1175/1520-0469(1979)036<1205:MFEITA>2.0.CO;2.

Cohen, J., and Coauthors, 2014: Recent Arctic amplification and extreme mid-latitude weather. *Nat. Geosci.*, **7**, 627–637, https://doi.org/10.1038/ngeo2234.

Comiso, J. C., 2006: Abrupt decline in the Arctic winter sea ice cover. *Geophys. Res. Lett.*, **33**, L18504, https://doi.org/10.1029/2006GL027341.

Dee, D. P., and Coauthors, 2011: The ERA-Interim reanalysis: Configuration and performance of the data assimilation system. *Quart. J. Roy. Meteor. Soc.*, **137**, 553–597, https://doi.org/10.1002/qj.828.

Diao, Y., J. Li, and D. Luo, 2006: A new blocking index and its application: Blocking action in the Northern Hemisphere. *J. Climate*, **19**, 4819–4839, https://doi.org/10.1175/JCLI3886.1.

Dole, R. M., and N. D. Gordon, 1983: Persistent anomalies of the extratropical Northern Hemisphere wintertime circulation: Geographical distribution and regional persistence characteristics. *Mon. Wea. Rev.*, **111**, 1567–1586, https://doi.org/10.1175/1520-0493(1983)111<1567:PAOTEN>2.0.CO;2.

Francis, J. A., and E. Hunter, 2007: Drivers of declining sea ice in the Arctic winter: A tale of two seas. *Geophys. Res. Lett.*, **34**, L17503, https://doi.org/10.1029/2007GL030995.

——, and S. J. Vavrus, 2012: Evidence linking Arctic amplification to extreme weather in mid-latitudes. *Geophys. Res. Lett.*, **39**, L06801, https://doi.org/10.1029/2012GL051000.

——, and ——, 2015: Evidence for a wavier jet stream in response to rapid Arctic warming. *Environ. Res. Lett.*, **10**, 014005, https://doi.org/10.1088/1748-9326/10/1/014005.

Graversen, R. G., T. Mauritsen, M. Tjernström, E. Källén, and G. Svensson, 2008: Vertical structure of recent Arctic warming. *Nature*, **451**, 53–56, https://doi.org/10.1038/nature06502.

Hassanzadeh, P., and Z. Kuang, 2015: Blocking variability: Arctic amplification versus Arctic Oscillation. *Geophys. Res. Lett.*, **42**, 8586–8595, https://doi.org/10.1002/2015GL065923.

Hoskins, B. J., I. N. James, and G. H. White, 1983: The shape, propagation and mean-flow interaction of large-scale weather systems. *J. Atmos. Sci.*, **40**, 1595–1612, https://doi.org/10.1175/1520-0469(1983)040<1595:TSPAMF>2.0.CO;2.

——, M. E. McIntyre, and A. W. Robertson, 1985: On the use and significance of isentropic potential vorticity maps. *Quart. J. Roy. Meteor. Soc.*, **111**, 877–946, https://doi.org/10.1002/qj.49711147002.

Illari, L., and J. C. Marshall, 1983: On the interpretation of eddy fluxes during a blocking episode. *J. Atmos. Sci.*, **40**, 2232–2242, https://doi.org/10.1175/1520-0469(1983)040<2232:OTIOEF>2.0.CO;2.

Kug, J.-S., J.-H. Jeong, Y.-S. Jang, B.-M. Kim, C. K. Folland, S.-K. Min, and S.-W. Son, 2015: Two distinct influences of Arctic warming on cold winters over North America and east Asia. *Nat. Geosci.*, **8**, 759–762, https://doi.org/10.1038/ngeo2517.

Lee, S., T. Gong, S. B. Feldstein, J. A. Screen, and I. Simmonds, 2017: Revisiting the cause of the 1989–2009 Arctic surface warming using the surface energy budget: Downward infrared radiation dominates the surface fluxes. *Geophys. Res. Lett.*, **44**, 10 654–10 661, https://doi.org/10.1002/2017GL075375.

Luo, B., D. Luo, L. Wu, L. Zhong, and I. Simmonds, 2017: Atmospheric circulation patterns which promote winter Arctic sea ice decline. *Environ. Res. Lett.*, **12**, 054017, https://doi.org/10.1088/1748-9326/aa69d0.

Luo, D., 2000: Planetary-scale baroclinic envelope Rossby solitons in a two-layer model and their interaction with synoptic-scale eddies. *Dyn. Atmos. Oceans*, **32**, 27–74, https://doi.org/10.1016/S0377-0265(99)00018-4.

——, 2005: A barotropic envelope Rossby soliton model for block–eddy interaction. Part I: Effect of topography. *J. Atmos. Sci.*, **62**, 5–21, https://doi.org/10.1175/1186.1.

——, and J. Li, 2000: Barotropic interaction between planetary- and synoptic-scale waves during the life cycles of blockings. *Adv. Atmos. Sci.*, **17**, 649–670, https://doi.org/10.1007/s00376-000-0026-5.

——, J. Cha, L. Zhong, and A. Dai, 2014: A nonlinear multiscale interaction model for atmospheric blocking: The eddy-blocking matching mechanism. *Quart. J. Roy. Meteor. Soc.*, **140**, 1785–1808, https://doi.org/10.1002/qj.2337.

——, Y. Xiao, Y. Yao, A. Dai, I. Simmonds, and C. L. E. Franzke, 2016a: Impact of Ural blocking on winter warm Arctic–cold Eurasian anomalies. Part I: Blocking-induced amplification. *J. Climate*, **29**, 3925–3947, https://doi.org/10.1175/JCLI-D-15-0611.1.

——, ——, Y. Diao, A. Dai, C. L. E. Franzke, and I. Simmonds, 2016b: Impact of Ural blocking on winter warm Arctic–cold Eurasian anomalies. Part II: The link to the North Atlantic Oscillation. *J. Climate*, **29**, 3949–3971, https://doi.org/10.1175/JCLI-D-15-0612.1.

——, X. Chen, and S. B. Feldstein, 2018: Linear and nonlinear dynamics of North Atlantic Oscillations: A new thinking of symmetry breaking. *J. Atmos. Sci.*, **75**, 1955–1977, https://doi.org/10.1175/JAS-D-17-0274.1.

McWilliams, J. C., 1980: An application of equivalent modons to atmospheric blocking. *Dyn. Atmos. Oceans*, **5**, 43–66, https://doi.org/10.1016/0377-0265(80)90010-X.

Mori, M., M. Watanabe, H. Shiogama, J. Inoue, and M. Kimoto, 2014: Robust Arctic sea-ice influence on the frequent Eurasian cold winters in past decades. *Nat. Geosci.*, **7**, 869–873, https://doi.org/10.1038/ngeo2277; Corrigendum, **8**, 159, https://doi.org/10.1038/ngeo2348.

Murray, R. J., and I. Simmonds, 1995: Responses of climate and cyclones to reductions in Arctic winter sea ice. *J. Geophys. Res.*, **100**, 4791–4806, https://doi.org/10.1029/94JC02206.

Nayfeh, A. H., 2000: *Perturbation Methods*. John Wiley and Sons, 437 pp.

Newson, R. L., 1973: Response of general circulation model of the atmosphere to removal of the Arctic ice-cap. *Nature*, **241**, 39–40, https://doi.org/10.1038/241039b0.

Outten, S. D., and I. Esau, 2012: A link between Arctic sea ice and recent cooling trends over Eurasia. *Climatic Change*, **110**, 1069–1075, https://doi.org/10.1007/s10584-011-0334-z.

Overland, J. E., M. Wang, and S. Salo, 2008: The recent Arctic warm period. *Tellus*, **60A**, 589–597, https://doi.org/10.1111/j.1600-0870.2008.00327.x.

——, K. R. Wood, and M. Wang, 2011: Warm Arctic—cold continents: Climate impacts of the newly open Arctic Sea. *Polar Res.*, **30**, 15787, https://doi.org/10.3402/polar.v30i0.15787.

Rex, D. F., 1950: Blocking action in the middle troposphere and its effect upon regional climate. I. An aerological study of blocking action. *Tellus*, **2**, 196–211, https://doi.org/10.1111/j.2153-3490.1950.tb00331.x.

Scherrer, S. C., M. Croci-Maspoli, C. Schwierz, and C. Appenzeller, 2006: Two-dimensional indices of atmospheric blocking and their statistical relationship with winter climate patterns in the Euro-Atlantic region. *Int. J. Climatol.*, **26**, 233–249, https://doi.org/10.1002/joc.1250.

Screen, J. A., and I. Simmonds, 2010: The central role of diminishing sea ice in recent Arctic temperature amplification. *Nature*, **464**, 1334–1337, https://doi.org/10.1038/nature09051.

——, and ——, 2013: Exploring links between Arctic amplification and mid-latitude weather. *Geophys. Res. Lett.*, **40**, 959–964, https://doi.org/10.1002/grl.50174.

Semenov, V. A., and M. Latif, 2015: Nonlinear winter atmospheric circulation response to Arctic sea ice concentration anomalies for different periods during 1966–2012. *Environ. Res. Lett.*, **10**, 054020, https://doi.org/10.1088/1748-9326/10/5/054020.

Serreze, M. C., M. M. Holland, and J. Stroeve, 2007: Perspectives on the Arctic's shrinking sea-ice cover. *Science*, **315**, 1533–1536, https://doi.org/10.1126/science.1139426.

Shepherd, T. G., 2016: Effects of a warming Arctic. *Science*, **353**, 989–990, https://doi.org/10.1126/science.aag2349.

Shutts, G. J., 1983: The propagation of eddies in diffluent jetstreams: Eddy vorticity forcing of 'blocking' flow fields. *Quart. J. Roy. Meteor. Soc.*, **109**, 737–761, https://doi.org/10.1002/qj.49710946204.

Simmonds, I., 2015: Comparing and contrasting the behaviour of Arctic and Antarctic sea ice over the 35 year period 1979–2013. *Ann. Glaciol.*, **56**, 18–28, https://doi.org/10.3189/2015AoG69A909.

——, and P. D. Govekar, 2014: What are the physical links between Arctic sea ice loss and Eurasian winter climate? *Environ. Res. Lett.*, **9**, 101003, https://doi.org/10.1088/1748-9326/9/10/101003.

Stroeve, J. C., M. C. Serreze, F. Fetterer, T. Arbetter, W. Meier, J. Maslanik, and K. Knowles, 2005: Tracking the Arctic's shrinking ice cover: Another extreme September minimum in 2004. *Geophys. Res. Lett.*, **32**, L04501, https://doi.org/10.1029/2004GL021810.

Tibaldi, S., and F. Molteni, 1990: On the operational predictability of blocking. *Tellus*, **42A**, 343–365, https://doi.org/10.3402/tellusa.v42i3.11882.

Tyrlis, E., and B. J. Hoskins, 2008: Aspects of a Northern Hemisphere atmospheric blocking climatology. *J. Atmos. Sci.*, **65**, 1638–1652, https://doi.org/10.1175/2007JAS2337.1.

Vautard, R., and B. Legras, 1988: On the source of midlatitude low-frequency variability. Part II: Nonlinear equilibration of weather regimes. *J. Atmos. Sci.*, **45**, 2845–2867, https://doi.org/10.1175/1520-0469(1988)045<2845:OTSOML>2.0.CO;2.

Vihma, T., 2014: Effects of Arctic sea ice decline on weather and climate: A review. *Surv. Geophys.*, **35**, 1175–1214, https://doi.org/10.1007/s10712-014-9284-0.

Walsh, J. E., 2014: Intensified warming of the Arctic: Causes and impacts on middle latitudes. *Global Planet. Change*, **117**, 52–63, https://doi.org/10.1016/j.gloplacha.2014.03.003.

Yao, Y., D. Luo, A. Dai, and I. Simmonds, 2017: Increased quasi stationarity and persistence of winter Ural blocking and Eurasian extreme cold events in response to Arctic warming. Part I: Insights from observational analyses. *J. Climate*, **30**, 3549–3568, https://doi.org/10.1175/JCLI-D-16-0261.1.

Yeh, T. C., 1949: On energy dispersion in the atmosphere. *J. Meteor.*, **6**, 1–16, https://doi.org/10.1175/1520-0469(1949)006<0001:OEDITA>2.0.CO;2.